Investigation of Vertical Mass Transport and Composition of the Mixed Gas in the Thermosphere

by

T. F. Johnsrud

B.S., University of Colorado Boulder, 2018

A thesis submitted to the

Faculty of the Graduate School of the

University of Colorado in partial fulfillment

of the requirements for the degree of

Master of Science

Department of Aerospace Engineering Sciences

2019

This thesis entitled:
Investigation of Vertical Mass Transport and Composition of the Mixed Gas in the Thermosphere
written by T. F. Johnsrud
has been approved for the Department of Aerospace Engineering Sciences

_____

Prof. Jeffrey Thayer

_____

Dr. Eric Sutton

_____

Prof. John Evans

Date _____

The final copy of this thesis has been examined by the signatories, and we find that both the content and the form meet acceptable presentation standards of scholarly work in the above mentioned discipline.

Johnsrud, T. F. (MS, Aerospace Engineering)

Investigation of Vertical Mass Transport and Composition of the Mixed Gas in the Thermosphere

Thesis directed by Prof. Jeffrey Thayer

To better deal with the difficult problem of satellite drag and orbit prediction, this thesis derives and presents an improved way of looking at vertical mass transport and composition in the thermosphere, as well illustrates why helium behaves inversely to the major neutral species in the thermosphere. Scale height analysis shows that helium concentrations at 400km can be related to large scale height perturbations from diffusive equilibrium. A study of molecular, thermal, and eddy diffusion show that the magnitude of the effect of each process varies according to the scale height perturbation from diffusive equilibrium, and that molecular diffusion dominates in the thermosphere, especially at high altitudes. Comparison against the atmospheric model TIEGCM show agreement with the derivation's implications for vertical winds and the inverse behavior of helium, while comparison with the MSIS model shows that an averaged empirical model does not have the fidelity necessary to resolve individual transport processes.

Acknowledgements

I would like to thank my advisor, Professor Jeffrey Thayer, for the effort he has put in towards guiding me along my educational career as well as the opportunities he has given me. Starting with my presentation at CEDAR in 2017, which was my first foray into research, Professor Thayer has provided opportunities to meet people who expand my knowledge and interest in the topics related to my thesis.

Contents

Chapter

Tables

Table

Figures

Figure

Chapter 1

Introduction

1.1 Background Motivation: Satellite Drag

The underlying motivation behind this research is the problem of satellite drag and orbit prediction. The main challenges when predicting satellite drag are knowing the atmospheric density as well as the coefficient of drag for the satellite. The total density has a direct bearing on the drag force, but the atmospheric composition will also change the coefficient of drag. Due to helium's high thermal velocity, the molecules are able to impinge on sides of the spacecraft not necessarily aligned with the ram velocity. This increases the drag coefficient for the spacecraft and illustrates why atmospheric composition also plays a role in the satellite drag problem.

The most populated satellite and space debris orbital region is in the Low Earth Orbit or LEO region which spans an altitude range of between 200-2000km. The thermosphere is a region of the atmosphere which extends above the altitude of minimum temperature called the mesopause which occurs in the 80-90km range [Prölss, 2004]. Figure 1.1 shows the temperature profile that defines the thermosphere. With an increased understanding of how the dynamics in the thermosphere evolve, better atmospheric composition and total density estimates can be made, increasing the fidelity of orbit prediction and drag modeling.

1.2 Previous Research and Purpose

Prieto et al. [2014] mentions it is common to calculate satellite acceleration due to drag as $a_{drag} = \frac{1}{2}\rho V^2 C_D \frac{S}{M}$ where ρ is the mass density of the atmosphere, V is the relative velocity of the

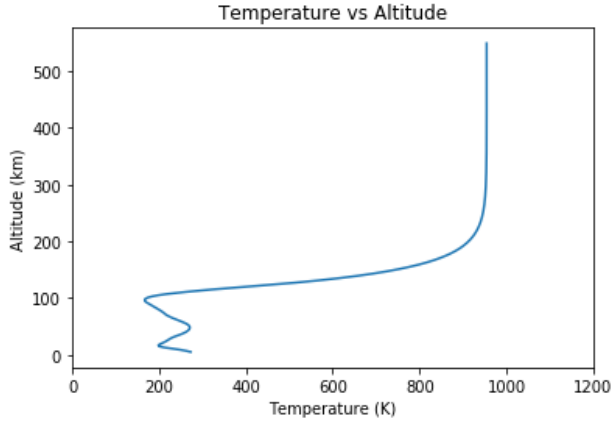

Figure 1.1: Temperature profile in the thermosphere from MSIS.

satellite and atmosphere, C_D is the coefficient of drag, S is the surface area of interaction, and m the mass of the satellite. While s and m can be known fairly accurately if the orientation of the satellite is known, uncertainties in the other three variables can significantly alter the acceleration estimate. Coefficient of drag is often assumed to be a value between 1.5 and 3 [Eberhard Gill, 2011, Pg. 95], and relative velocity is difficult to exactly predict due to the presence of atmospheric winds. As mentioned previously, the C_D estimate improves when knowledge of what gas-surface interactions are taking place, which is why predicting the atmospheric composition, especially the presence of helium, is important.

The idea of studying atmospheric composition and density is not a new concept. Ever since scientific satellites were first launched, atmospheric readings and data was collected. As far back as 1961 helium was experimentally confirmed to be present in the atmosphere using spectroscopic techniques, and it was also determined to be necessary to fit atmospheric drag data to the satellite Echo 1 [Kockarts, 1973]. Due to the difficulty of obtaining insitu measurements however, little data exists from direct readings. As satellites pass through parts of the thermosphere, they can take readings, however these are isolated to local areas and times, which makes it challenging to build accurate atmospheric models around. Many researchers have taken to explaining various features present in the thermosphere and ionosphere with data gathered indirectly then, with lidar measurements, satellite drag data, and the limited amount of insitu measurements. Phenomena such

as the winter helium bulge, equatorial thermospheric anomaly, neutral thermospheric composition, and mixing methods for the thermosphere have all been studied extensively.

The purpose of this research is to provide a robust mathematical model for the the mixing and transport of neutral gasses in the thermosphere and compare it to what is observed in the MSIS and TIEGCM thermospheric models. Additionally, while helium is often overlooked in the consideration of constituent gasses due to it's small presence in the atmospheric composition, this thesis aims to show that it plays a dynamic role. From studying helium and its response in relation to other neutral species, a greater understanding of the underlying dynamics for the entire thermosphere can be reached.

Chapter 2

Model Background

This research used two thermospheric models to evaluate the predictions and observations made by the mathematical model presented in Chapter 3, the Naval Research Laboratory Mass Spectrometer and Incoherent Scatter radar model, or MSIS, and the National Center for Atmospheric Research - Thermosphere Ionosphere Electrodynamics General Circulation Model, or TIEGCM.

2.1 MSIS

MSIS is an empirical model of the atmosphere which draws on data collected over decades from many projects. It was initially developed in 1977 as an upper thermospheric model, but since then several updates were made as more data was obtained. In 1983 rocket data expanded the model to the lower thermosphere, and in 1990 it was extended all the way to ground. The current version, and the one used for this research is NRLMSISE-00, which was released in 2000 with updates made from more satellite drag data and other modifications [Picone et al., 2002].

Input parameters to MSIS include the date and time; geodetic altitude, longitude, and latitude; and also parameters that help estimate the state of the atmosphere such as a_p, a geomagnetic index, and F10.7, a measure of solar activity. F10.7 is used as an indicator of how much solar energy is being absorbed by the ionosphere. It cycles with the eleven year solar cycle, which has a significant impact on the range and expansion of the thermosphere. For plots made in this paper, an F10.7 value of 188 was used in order to match the results with the TIEGCM model as

best as possible which was run at an F10.7 value of 180. This corresponds with a solar maximum coincidentally.

2.2 TIEGCM

In contrast to the empirical approach used by MSIS, TIEGCM solves for atmospheric variables using a physics based approach. Although being one of the most common and robust physics based model of the thermosphere currently available, it is not the first or only one to have existed. The University College at London - Thermospheric General Circulation Model and the NCAR - Thermospheric General Circulation Model were both developed in the early 80s, and regional ionospheric models were developed to describe specific sections of the ionosphere [Wang, 1998]. In 1988 the coupled thermospheric/ionospheric NCAR-TIEGCM model was first created, and since this time has been updated and modified to reflect further understandings of the upper atmospheric environment.

For the purpose of this paper, TIEGCM numerically solves the momentum, continuity, and energy equations over a mesh encompassing the globe. The grid used for this research is a 2.5° latitude and longitude grid, with 57 pressure levels in the vertical direction. TIEGCM solves along pressure isosurfaces in order to simplify the equations and reduce errors associated with interpolating a fixed altitude grid onto the fluctuating atmosphere. Pressure coordinates present themselves as a natural coordinate system for the solver due to the pressure term in the momentum equation. The dataset used in this research comes from Hsu [2016] and the model runs she performed. It is a run of the model until it reaches a diurnally reproducible state, such that any transient effects became periodic to match with the day-night cycle of the model. The simulation was run with a high solar activity, $F10.7 = 180$, low geomagnetic activity, under equinox conditions, and the ion-drag term was included. Table 2.1 shows the file used and description from Hsu.

Table 2.1: TIEGCM run and description for data used in this thesis.

Filename	`HSUVW.tiegcm2.0_dres.pdrag_f107_180_001.nc`
TIEGCM Version	2.0
Resolution	2.5 x 2.5
Description	Full simulation at solar max (with field-aligned ion drag and with frictional heating)

Chapter 3

Mathematical Derivation

In order to predict the gas dynamics inside the thermosphere, a governing equation describing the transport of constituent species in the vertical (z) direction was derived from first principles. This derivation is based on work from presented in [Liu, 2013]. Going through the derivation shows the fundamental principles behind the governing equation, and it gives insight into the physical meaning of the final form. First, Table 3.1 defines terms and nomenclature used.

Table 3.1: Definition of terms used in the mathematical derivation of the species transport equation.

Term	Meaning	Units
$\vec{U}$	Mass averaged velocity	$\left[\frac{m}{s}\right]$
$\vec{U_i}$	Individual species mean velocity	$\left[\frac{m}{s}\right]$
$\vec{C_i} = \left(\vec{U_i} - \vec{U}\right)$	Individual species diffusion velocity	$\left[\frac{m}{s}\right]$
ν_{it}	Momentum weighted collision frequency of species $i \rightarrow t$	$\left[\frac{1}{s}\right]$
$D_i = \frac{kT}{\sum_{t \neq i} m_i \nu_{it}}$	Molecular diffusion coefficient	$\left[\frac{m^2}{s}\right]$
ρ	Total mass density	$\left[\frac{kg}{m^3}\right]$
ρ_i	Individual species mass density	$\left[\frac{kg}{m^3}\right]$
$H = -x\frac{1}{\frac{\partial x}{\partial z}}$	Scale height of variable x, decreasing with height	[m]
$\frac{\rho_i}{\rho}$	Mass mixing ratio	N/A
m_i	Molecular weight of species 'i'	$\frac{kg}{molecule}$

3.1 Transport Equation

The following derivation stems from three equations, the mass continuity equation for an individual species, mass continuity for the whole gas mixture, and the gas species vertical momentum equation. These are outlined in equations 3.1, 3.2, and 3.3 respectively.

$$\frac{\partial \rho_i}{\partial t} + \vec{\nabla} \cdot \left(\rho_i \vec{U_i}\right) = S_i - L_i \tag{3.1}$$

$$\frac{\partial \rho}{\partial t} + \vec{\nabla} \cdot \left(\rho \vec{U}\right) = 0 \tag{3.2}$$

$$\frac{\partial P_i}{\partial z} + \rho_i g = -\rho_i \sum_{t \neq i} \nu_{it} \left(\vec{C_i} - \vec{C_t}\right) \tag{3.3}$$

Because the Navier-Stokes equation is being used here, it is useful to define the altitude range for which the derivation can be considered valid. The NS equation requires an assumption of a continuous fluid. This is characterized by Knudsen number $Kn = \frac{\lambda}{L}$ where λ is the mean free path of the gas, and L is a characteristic length. Figure 3.1 shows the Knudsen number for the atmosphere from MSIS. As $Kn < 1$ is generally used for the continuum assumption, the following derivation is valid up to 400-600km depending on the atmospheric conditions because the length scale used is a scale height which is on the order of tens of kilometers.

Moving to the derivation, Equation 3.1 says that for an individual gas species, the time rate of change of the mass density plus the divergence of the mass density flux is balanced by the net of the source and loss terms on the right hand side. By subtracting $\vec{\nabla} \cdot \left(\rho_i \vec{U}\right) = \vec{\nabla}\left(\frac{\rho_i}{\rho}\right) \cdot \left(\rho \vec{U}\right) + \frac{\rho_i}{\rho}\left(\vec{\nabla} \cdot (\rho \vec{U})\right)$ from both sides of 3.1 and combining the divergence operations on the left hand side, the following representation of the individual mass continuity equation can be found:

$$\frac{\partial \rho_i}{\partial t} + \vec{\nabla} \cdot \left[\rho_i \left(\vec{U_i} - \vec{U}\right)\right] = S_i - L_i - \rho \vec{U} \cdot \vec{\nabla}\left(\frac{\rho_i}{\rho}\right) - \frac{\rho_i}{\rho} \vec{\nabla} \cdot \left(\rho \vec{U}\right) \tag{3.4}$$

From this form, the Equation 3.2 can be applied along with bringing in the definition of species diffusion velocity $\vec{C_i}$ to describe the time rate of change of the mass mixing ratio in Equation 3.5.

$$\rho \frac{\partial}{\partial t}\left(\frac{\rho_i}{\rho}\right) = -\vec{\nabla} \cdot \left[\rho_i \vec{C_i}\right] + S_i - L_i - \rho \vec{U} \cdot \vec{\nabla}\left(\frac{\rho_i}{\rho}\right) \tag{3.5}$$

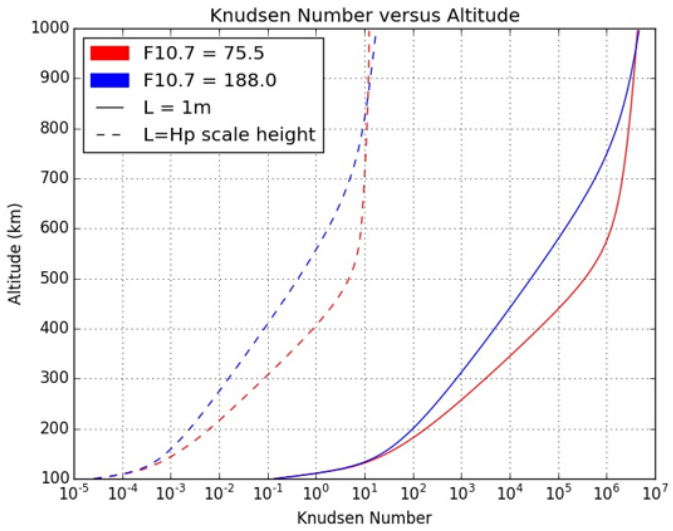

Figure 3.1: MSIS derived Knudsen numbers.

Using the reverse chain rule to pull ρ into the time derivative conveniently expresses the equation in terms of the mass mixing ratio, $\frac{\rho_i}{\rho}$. This can then be arranged to form the material derivative of the mass mixing ratio by bringing the convective gradient to the left hand side. The governing equation for a gas species in the thermosphere is then shown to be Equation 3.6.

$$\rho \frac{D}{Dt}\left(\frac{\rho_i}{\rho}\right) = -\vec{\nabla} \cdot [\rho_i \vec{C_i}] + S_i - L_i \tag{3.6}$$

In the thermosphere, the source and loss terms are negligible for the neutral gasses, thus the material derivative is solely dependent on the gradient of the diffusive mass flux $\vec{\nabla} \cdot [\rho_i \vec{C_i}]$, which has several components and is derived below.

3.2 Diffusion

The most basic definition for the diffusive mass flux of one gas through a mixture is the density times the diffusion velocity of the gas, or $\Gamma_i = \rho_i \vec{C_i}$. The first form of diffusion considered here is molecular diffusion, present when there is a concentration gradient for a constituent gas species. From Equation 3.3, if only the vertical direction is considered, then $C_i^z = \frac{1}{\rho_i \sum_{t \neq i} \nu_{it}} \big(- \frac{\partial P_i}{\partial z} - \rho_i g + \rho_i \sum_{t \neq i} \nu_{it} C_t^z \big)$. Taking the expression for the molecular diffusion coefficient and substituting it into

the expression for C_i^z simplifies to $C_i^z = \frac{D_i}{\rho_i}\big(- \frac{m_i}{kT}\frac{\partial P_i}{\partial z} - \frac{m_i}{kT}\rho_i g + \frac{m_i}{kT}\rho_i \sum_{t\neq i} \nu_{it} C_t^z\big)$. The diffusive flux equation can then be expanded with the ideal gas law to Equation 3.7. Note that the gradient $\frac{\partial m_i}{\partial z}$ is equal to zero due to the molecular mass of a molecule being constant. Equation 3.7 differs from what is presented in Liu [2013] by a sign change on the summation term, and Appendix A.1 goes through the derivation and shows where the difference arises.

$$\Gamma_i^M = \rho_i C_i^z = -D_i\big(\frac{\partial \rho_i}{\partial z} + \frac{\rho_i}{T}\frac{\partial T}{\partial z} + \frac{\rho_i m_i g}{kT} - \frac{\rho_i m_i}{kT}\sum_{t\neq i}\nu_{it}C_t^z\big) \tag{3.7}$$

A second form of diffusion, thermal diffusion, becomes significant for lighter species in the gas mixture such as helium and hydrogen. This is due to the fact that unlike gasses will diffuse under a temperature gradient [Richmond, 1983] and is discussed in the next chapter. This effect, given by $\Gamma_i^T = -\rho_i D_{Ti}\frac{1}{T}\frac{\partial T}{\partial z}$, can be added to the expression for molecular diffusion shown in Equation 3.7 to capture the effects of both processes. This is shown in Equation 3.8, where α_i is now the ratio of diffusion coefficients, $\frac{D_{Ti}}{D_i}$.

$$\begin{aligned}
\Gamma_i &= -D_i\big(\frac{\partial \rho_i}{\partial z} + \frac{\rho_i}{T}\frac{\partial T}{\partial z} + \frac{\rho_i m_i g}{kT} - \frac{\rho_i m_i}{kT}\sum_{t\neq i}\nu_{it}C_t^z\big) - \rho_i D_{Ti}\frac{1}{T}\frac{\partial T}{\partial z} \quad \text{or equivalently} \\
\Gamma_i &= -\rho_i D_i\big(\frac{1}{\rho_i}\frac{\partial \rho_i}{\partial z} + \frac{(1+\alpha_i)}{T}\frac{\partial T}{\partial z} - \frac{m_i g}{kT} + \frac{m_i}{kT}\sum_{t\neq i}\nu_{it}C_t^z\big)
\end{aligned} \tag{3.8}$$

The third and final form of diffusion being considered in this region of the atmosphere is eddy diffusion. This is the effect of turbulence in the atmosphere to mix the gas species, and is generally negligible in the thermosphere. This process, which drives the mixture towards uniformity and homogenization, rapidly falls off above 100km in the region denoted as the turbopause due to the increasing effect of viscosity damping turbulent motions. The eddy diffusive mass flux is adapted from the molecular eddy diffusive flux equation in $\phi_i^\epsilon = -Kn\frac{d}{dz}\big(\frac{n_i}{n}\big)$ where K is the eddy diffusion coefficient [Prölss, 2004]. Changing from number density to mass density and distributing the derivative leads to Equation 3.9 for the mass flux due to eddy diffusion.

$$\Gamma_i^E = -K\rho\frac{d}{dz}\big(\frac{\rho_i}{\rho}\big) = -\rho_i K\big(- \frac{1}{\rho}\frac{\partial \rho}{\partial z} + \frac{1}{\rho_i}\frac{\partial \rho_i}{\partial z}\big) \tag{3.9}$$

Combining the effects of molecular diffusion due to density gradients, thermal diffusion resulting from temperature gradients, and eddy diffusion from turbulent mixing results in the final

expression for the species diffusive mass flux in the thermosphere shown in Equation 3.10.

$$\Gamma_i = -\rho_i D_i\big(\frac{1}{\rho_i}\frac{\partial \rho_i}{\partial z} + \frac{1}{T}\frac{\partial T}{\partial z} + \frac{m_i g}{kT} - \frac{m_i}{kT}\sum_{t\neq i}\nu_{it}C_t^z\big) - \rho_i D_{Ti}\frac{1}{T}\frac{\partial T}{\partial z} - \rho_i K\big(\frac{1}{\rho_i}\frac{\partial \rho_i}{\partial z} - \frac{1}{\rho}\frac{\partial \rho}{\partial z}\big) \quad (3.10)$$

3.3 Using Scale Heights

A useful tool in simplifying and analyzing these equations is the use of scale heights. Table 3.1 shows the general definition of a scale height for a parameter that decreases in value with altitude and it is immediately apparent that terms of this form appear frequently in Equation 3.10. Defining all of these terms in relation to their scale height results in the definitions given in Equation 3.11.

$$\begin{aligned} \frac{1}{H^*_{\rho i}} &= -\frac{1}{\rho_i}\frac{\partial \rho_i}{\partial z}, & \frac{1}{H_\rho} &= -\frac{1}{\rho}\frac{\partial \rho}{\partial z}, & \frac{1}{H_m} &= -\frac{1}{m}\frac{\partial m}{\partial z} \\ \frac{1}{H_T} &= \frac{1}{T}\frac{\partial T}{\partial z}, & \frac{1}{H_P} &= -\frac{1}{P}\frac{\partial P}{\partial z}, & \frac{1}{H_{Pi}} &= -\frac{1}{P_i}\frac{\partial P_i}{\partial z} \end{aligned} \quad (3.11)$$

A second, more useful expression for $\frac{1}{H_{Pi}}$ and $\frac{1}{H_P}$ can be derived when combined with the ideal gas law and the assumption of diffusive or hydrostatic equilibrium respectively. Looking at Equation 3.3, in order to satisfy momentum conservation it can be seen that if the atmosphere is in diffusive equilibrium, the $\big(\vec{C_i} - \vec{C_t}\big)$ term becomes zero because the diffusive velocities are both zero. This means $\frac{\partial P_i}{\partial z} + \rho_i g = 0$ which is an individual species analogue to the hydrostatic equilibrium equation $\frac{\partial P}{\partial z} + \rho g = 0$. Taken together with the ideal gas law, these equations result in the simplifications shown in Equation 3.12 for pressure scale heights under diffusive or hydrostatic equilibrium.

$$\frac{1}{H_{Pi}} = -\frac{1}{P_i}\frac{\partial P_i}{\partial z} = \frac{m_i g}{kT} \quad \text{and} \quad \frac{1}{H_P} = -\frac{1}{P}\frac{\partial P}{\partial z} = \frac{mg}{kT} \quad (3.12)$$

Similarly, using the ideal gas law, $\rho = \frac{Pm}{RT}$ where m is the mean molecular mass of the gas and R is the universal gas constant, the inverse scale height expression for ρ and ρ_i can be rewritten under the assumption of hydrostatic or diffusive equilibrium. Applying the product rule and quotient rule for the z derivative can be shown to be $\frac{1}{\rho}\frac{\partial \rho}{\partial z} = -\frac{1}{T}\frac{\partial T}{\partial z} + \frac{1}{m}\frac{\partial m}{\partial z} + \frac{1}{P}\frac{\partial P}{\partial z}$. This results in Equation 3.13 relating the scale heights of the atmospheric parameters.

$$\frac{1}{H_\rho} = \frac{1}{H_P} + \frac{1}{H_T} + \frac{1}{H_m} = \frac{mg}{kT} + \frac{1}{H_T} + \frac{1}{H_m} \quad (3.13)$$

Because the total atmospheric gas is considered to be in hydrostatic equilibrium, this definition holds. A similar process produces the Equation 3.14 for the relationship between scale heights for an individual gas species under diffusive equilibrium. Since for an individual species the mean molecular mass is constant, the third term of Equation 3.13 is dropped.

$$\frac{1}{H_{\rho_i}} = \frac{m_i g}{kT} + \frac{1}{H_T} \tag{3.14}$$

The difference between $H_{\rho i}$ and $H^*_{\rho i}$ is that $H_{\rho i}$ is the mass density scale height for a gas species in diffusive equilibrium and $H^*_{\rho i}$ is the actual mass density scale height of the gas species in the thermosphere.

Applying the scale height definitions to Equation 3.10 results in a form that is easier to understand shown in Equation 3.15.

$$\Gamma_i = \rho_i C_i^z = -\rho_i D_i \big(\frac{1}{H_{\rho i}} - \frac{1}{H^*_{\rho i}} - \frac{m_i}{kT}\sum_{t\neq i}\nu_{it}C_t^z\big) - \rho_i D_{Ti}\frac{1}{H_T} - \rho_i K\big(\frac{1}{H_\rho} - \frac{1}{H^*_{\rho i}}\big) \tag{3.15}$$

Considering the transport of species i, the molecular diffusion term is modified by the perturbation of the species mass density scale height from diffusive equilibrium as well as the pressure term created by the diffusive velocities of other species. If the species is in diffusive equilibrium the scale height terms will cancel. Thermal diffusion is always present under a temperature gradient, and eddy diffusion is modified by the perturbation of the species scale height from the total atmospheric scale height. This characteristic of eddy diffusion describes how it drives the mixture to be homogeneous, with the species concentration scale heights matching the total. This also has a reverse effect depending on the species. For a species such as N2, which generally has a scale height lower than that of the average, the effect of eddy diffusion is opposite that of helium, which has a scale height larger than that of the total atmosphere.

3.4 Expanded Transport Equation

Recall that $\rho\frac{D}{Dt}\left(\frac{\rho_i}{\rho}\right) = -\vec{\nabla}\cdot[\rho_i\vec{C}_i]$ is the mass transport equation derived earlier with the negligible source and loss terms dropped. Restricting the derivatives to the z-component only

results in Equation 3.16.

$$\rho \frac{D}{Dt}\left(\frac{\rho_i}{\rho}\right) = -\frac{\partial}{\partial z}(\rho_i C_i^z) \tag{3.16}$$

Expanding this with the result from 3.15 gives 3.17.

$$\rho \frac{D}{Dt}\left(\frac{\rho_i}{\rho}\right) = \frac{\partial}{\partial z}\left[\rho_i D_i\left(\frac{1}{H_{\rho i}} - \frac{1}{H^*_{\rho i}} - \frac{m_i}{kT}\sum_{t\neq i}\nu_{it}C_t^z\right) + \rho_i D_{Ti}\frac{1}{H_T} + \rho_i K\left(\frac{1}{H_\rho} - \frac{1}{H^*_{\rho i}}\right)\right] \tag{3.17}$$

Switching from the Lagrangian description to the Eulerian is helpful in some cases. This can be done by moving the convective derivative to the right hand side. Realizing that the convective derivative can also be expressed in terms of scale heights because $\rho w \frac{\partial}{\partial z}\left(\frac{\rho_i}{\rho}\right) = \rho_i w\left(-\frac{1}{\rho}\frac{\partial \rho}{\partial z} + \frac{1}{\rho_i}\frac{\partial \rho_i}{\partial z}\right) = \rho_i w\left(\frac{1}{H_\rho} - \frac{1}{H^*_{\rho i}}\right)$, where w is the z-component of velocity in the thermosphere called the vertical winds produces Equation 3.18.

$$\rho \frac{\partial}{\partial t}\left(\frac{\rho_i}{\rho}\right) = \frac{\partial}{\partial z}\left[\rho_i D_i\left(\frac{1}{H_{\rho i}} - \frac{1}{H^*_{\rho i}} - \frac{m_i}{kT}\sum_{t\neq i}\nu_{it}C_t^z\right) + \rho_i D_{Ti}\frac{1}{H_T} + \rho_i K\left(\frac{1}{H_\rho} - \frac{1}{H^*_{\rho i}}\right)\right] - \rho_i w\left(\frac{1}{H_\rho} - \frac{1}{H^*_{\rho i}}\right) \tag{3.18}$$

This is the form that the rest of this paper will refer to. The roles and magnitudes of the terms will be examined in the coming chapters to determine the dominant processes governing the species transport. As a final note, the effects of vertical winds has a similar property to eddy diffusion in that it works in opposite ways for different species. This means, for example, that helium and N2 mass mixing ratios have opposite responses to the presence of vertical winds.

Because the mass mixing ratio is prevalent in Equation 3.18 and its derivation, Figure 3.2 shows the plotted mass mixing ratio of several neutral species with altitude. At the lower altitudes, N_2 dominates, and is then surpassed by O_1. The mass mixing ratio for helium does not rise significantly until above 400km. For this reason, helium fluctuations in the lower thermosphere have little effect on the total mass continuity of the gas mixture.

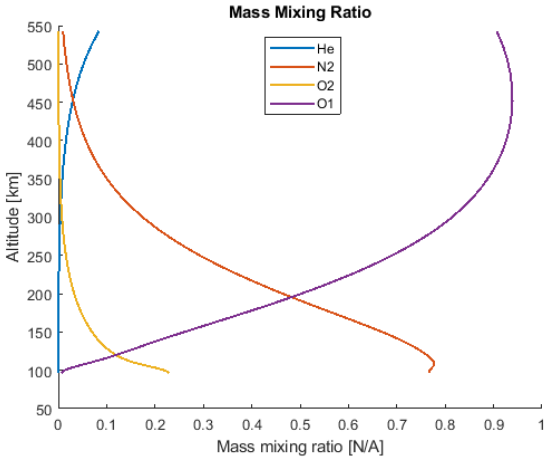

Figure 3.2: The mass mixing ratios of various neutral species in the thermosphere. TIEGCM run, UT = 0.03hr LT = 6.7hr latitude = 63.75.

Chapter 4

Scale Height Analysis

4.1 Comparison With Diffusive Equilibrium

Densities can be derived from the scale heights using Equation 4.1 where ρ_0 is the density known at some initial lower altitude, z_0.

$$\rho(z) = \rho_0 \exp\big(\int_{z_0}^{z} -\frac{z}{H_\rho(z)} dz\big) \tag{4.1}$$

The result is that $\rho(z)$ is an integrated quantity and a change in the scale height, even a slight difference, can have large effects once integrated over large altitude ranges. As shown in Chapter 3, the density scale heights of each species and the total gas are driving factors determining the transport of constituent gasses in the thermosphere. Equation 3.18 shows that for the diffusive and convective terms, the relationship between the actual species scale height and the diffusive equilibrium scale heights plays an important role. The scale height difference that causes diffusion also significantly alters the concentrations of a gas species at altitude. This can be seen at points over the globe, as illustrated in Figure 4.1 which shows the helium and nitrogen mass concentrations at 400km from the TIEGCM run with the magnetic equator overlayed in red. The profiles show a distinct inverse relationship. A closer look at the helium plot also shows features that follow the magnetic equator. On the northern and southern sides, there is an area of higher concentration separated by a trough where the equator lies. This can be attributed to the atmospheric circulation patterns induced from field aligned ion drag in the Equatorial Thermospheric Anomaly [Hsu et al., 2014]. Ions in the thermosphere interact with the magnetic field, transferring momentum and

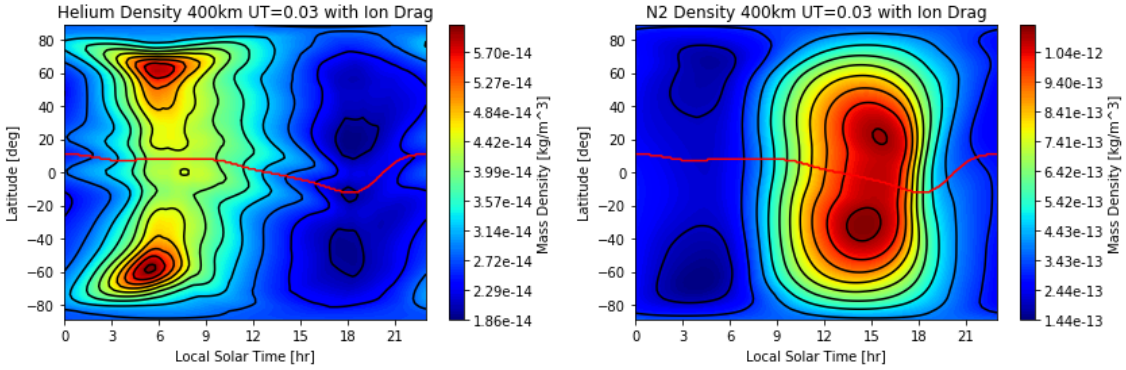

(a) (b)

Figure 4.1: Helium and Nitrogen mass density profiles at 400km. TIEGCM run, UT = 0.03

causing upward vertical winds at the magnetic equator and downward vertical winds on either side. Helium's large scale height difference from the atmospheric total drives it to respond to these vertical winds.

To examine the distinct helium and nitrogen enhancement regions, the scale heights of species are plotted in 4.2, 4.3, and 4.4 which correspond to latitudes of 63.75°, 58.75°, or 11.25° and solar local times of 6.7hr, 2.7hr, or 14hr respectively. Figure 4.2 is the location of the Northern helium enhancement and there is clearly an anomaly of the scale height. While oxygen and nitrogen follow their respective diffusive profiles closely, helium has a low altitude spike which indicates a persistence in mass density where the diffusive equilibrium profile would drop off. This low altitude feature in the scale height is enough to clearly create the high concentration seen at 400km. This reinforces the idea behind helium being loosely decoupled from the continuity equation, especially at lower altitudes where the more prevalent and heavier species make up the majority of the atmosphere. The heaviest, most prevalent species satisfy the mass transport, while large changes of helium concentrations have a small effect on the total gas. A second point of note is that N_2 and O_2 are species with a scale height less than that of the total atmosphere. From the $\frac{1}{H_\rho} - \frac{1}{H^*_{\rho i}}$ component in the eddy diffusion and vertical wind terms of Equation 3.18, this shows that the eddy diffusive and vertical winds response of nitrogen and molecular oxygen is the opposite that of atomic oxygen and

helium. Also, since helium scale height deviates so greatly from the total atmosphere, the vertical wind term has a significant effect on its mixing ratio in the thermosphere. Figure 4.3 is a location chosen where the 400km helium density is between that of the highest and lowest in Figure 4.1a. Again, while oxygen and nitrogen follow diffusive equilibrium profiles, helium clearly diverges. This persistent pattern suggests that helium is rarely in diffusive equilibrium which can be caused by it's sensitivity to vertical winds, perturbations at low altitudes, or other external factors. Figure 4.4 shows the scale heights at a point where nitrogen is heavily concentrated in Figure 4.1b. Helium is much closer to its diffusive profile, and the spike seen earlier is completely gone. While the scale heights of nitrogen and oxygen do not diverge much, helium clearly is a dynamic species in the thermosphere.

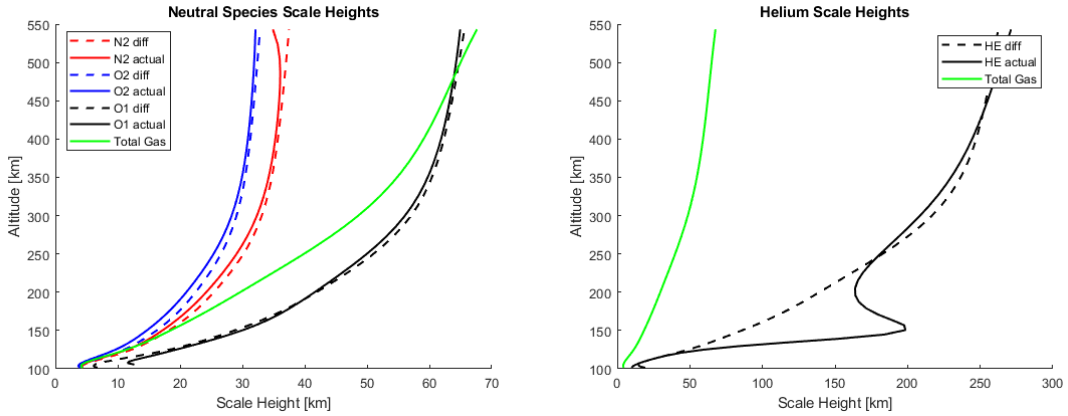

(a) (b)

Figure 4.2: Species mass density scale heights with equilibrium scale height and total atmospheric scale height for reference. TIEGCM run, UT = 0.03hr LT = 6.7hr latitude = 63.75.

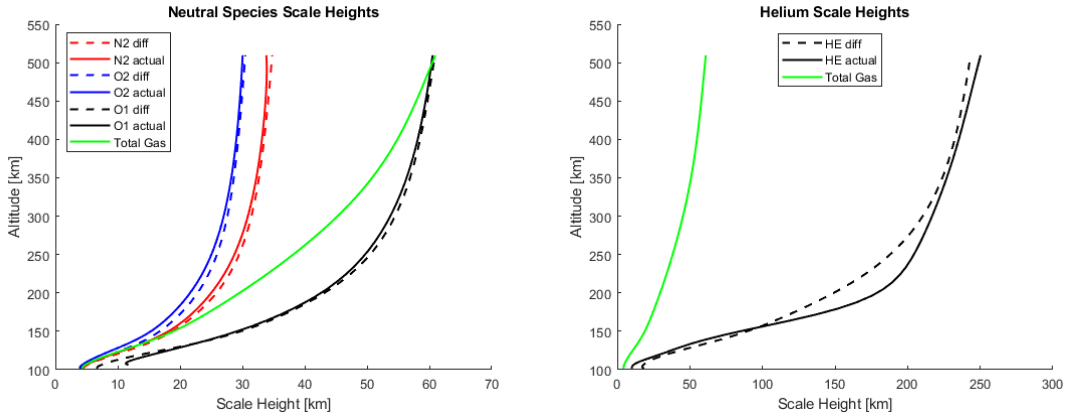

(a) (b)

Figure 4.3: Species mass density scale heights with equilibrium scale height and total atmospheric scale height for reference. TIEGCM run, UT = 0.03hr LT = 2.7hr latitude = 58.75.

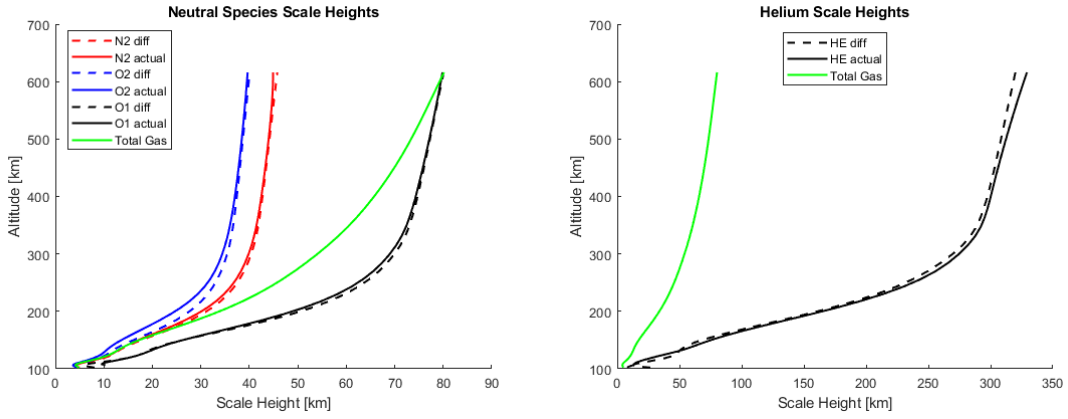

(a) (b)

Figure 4.4: Species mass density scale heights with equilibrium scale height and total atmospheric scale height for reference. TIEGCM run, UT = 0.03hr LT = 14hr latitude = 11.25.

4.2 Thermal Diffusion

The high thermal velocity of helium relative to the heavier species like O_2 and N_2 means that it is the only species to be significantly affected by thermal diffusion. A temperature gradient in the atmosphere also produces thermal velocity gradient for the molecules. This velocity gradient is largest for helium due to its small molecular weight, and it drives the gas to diffuse through the other gasses. Therefore, of the neutral species in the thermosphere, the effects of thermal diffusion are only significant for helium [Richmond, 1983]. Recall that α is defined as the ratio of the thermal diffusion coefficient to the molecular diffusion coefficient. Typical values for helium's α lie around -.38, this being the value used by Sutton et al. [Sutton et al., 2015]. Richmond states that the 1976 U.S. Standard Atmosphere uses a value of -.40. For the work done here, a value of -.38 is used for consistency with previous work.

Figure 4.5 shows how accounting for thermal diffusion changes the equilibrium profile of helium in the thermosphere. At lower altitudes, the contribution of thermal diffusion is significant,

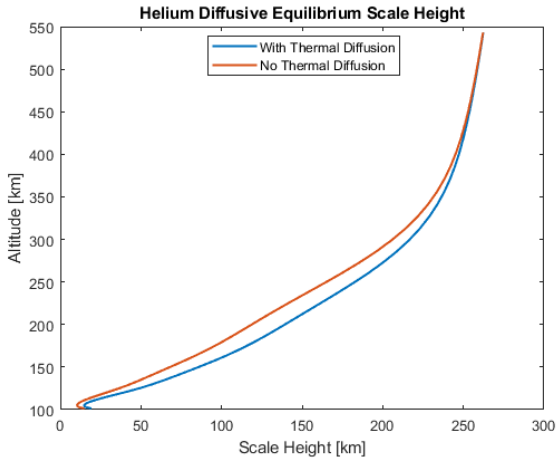

Figure 4.5: Differences in equilibrium scale height profiles for Helium when accounting for thermal diffusion. TIEGCM run, UT = 0.03hr LT = 6.7hr latitude = 63.75.

such that it changes the diffusive equilibrium scale height profile noticeably. After 350km however, the temperature gradient that sustains diffusion rapidly drops off and the two lines fall on top of each other.

Although the difference appears small, inputting the scale heights to the $exp\big(\int_{z_0}^{z} -\frac{z}{H_\rho(z)}dz\big)$ portion of Equation 4.1 produces significantly different values however. Table 4.1 shows the compared values of $exp\big(\int_{z_0}^{\sim 400km} -\frac{z}{H_\rho(z)}dz\big)$ when accounting for thermal diffusion versus without.

Table 4.1: Integrated effect of thermal diffusion on helium mass density at 400km.

Location	With Thermal Diffusion	Without Thermal Diffusion
Northern helium enhancement	0.052	0.027
Nitrogen enhancement	0.061	0.029

This means given the same ρ_0, the diffusive profile of helium without accounting for thermal diffusion produces roughly half the mass density as the profile that accounts for thermal diffusion.

4.3 MSIS Compared to TIEGCM

The results of the previous section show an interesting anti-correlation between nitrogen and helium. The physics based TIEGCM run predicts this, but the empirically assembled MSIS model also shows similar results. Figure 4.6 shows helium mass density at 400km in the same way Figure 4.1a does.

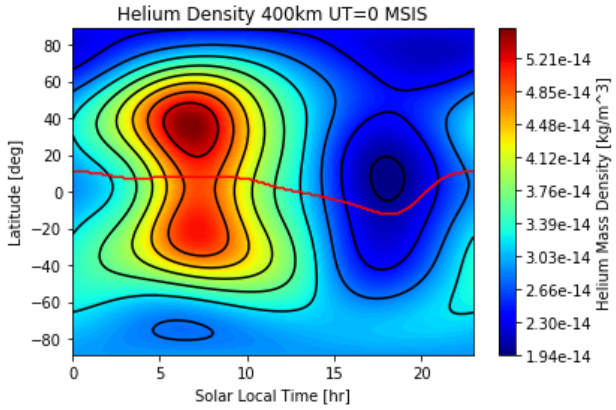

Figure 4.6: MSIS Helium mass density at 400km

Clear differences are apparent due to the smoothing and averaging done in the MSIS model, but the large scale features are consistent. Comparing the scale height results is less similar however. Figure 4.7 shows MSIS does not have the resolution or differentiation required to examine the scale heights in the way that TIEGCM does. The profiles of each species follow their equilibrium profiles nearly identically.

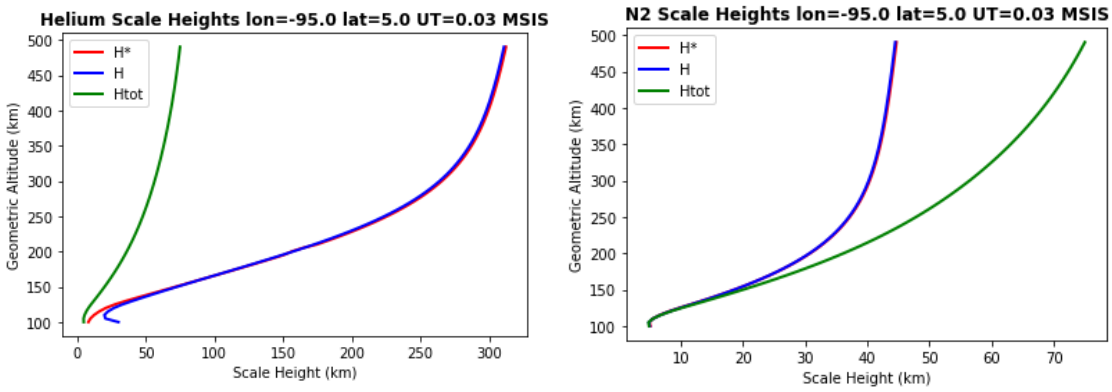

(a)

(b)

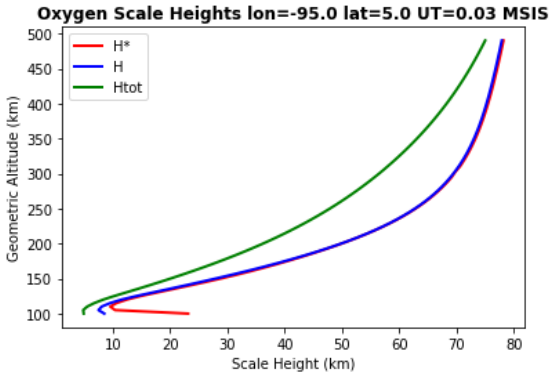

(c)

Figure 4.7: Species mass density scale heights with equilibrium scale height and total atmospheric scale height for reference.

Chapter 5

Mixing Magnitudes

In order to examine and compare the roles of turbulent and molecular diffusion processes as well as vertical wind transport, the magnitudes of the coefficients can be examined. Recall that the molecular diffusion coefficient D_i depends on the collision frequency of species i with the rest of the gas mixture, as well as the molecular weight of species i. The collision frequency of species i with species t can be calculated from the Equations in 5.1 [Schunk and Nagy, 2000]. This characterizes the momentum transfer weighted interactions of two species, and it can be shown that $\nu_{it} n_i m_i = \nu_{ti} n_t m_t$.

$$\begin{aligned}
\nu_{it} &= \frac{16}{3} \frac{n_t m_t}{m_i + m_t} \Omega_{it} \\
\Omega_{it} &= \frac{\alpha}{\sqrt{4\pi}} Q_{it} \\
\alpha^2 &= \frac{2kT_{it}}{\mu_{it}} \\
\mu_{it} &= \frac{m_i m_t}{m_i + m_t} \\
T_{it} &= \frac{m_i T_t + m_t T_i}{m_i + m_t} \\
Q_{it} &= \pi \sigma^2
\end{aligned} \tag{5.1}$$

Where T is the temperature of the interacting species, k is Boltzmann's constant, and σ is the sum of the species collision radii. Combined with Equation 5.2, the diffusion coefficient for a given species can be calculated.

$$D_i = \frac{kT}{m_i \sum_{i \neq t} \nu_{it}} \tag{5.2}$$

The eddy diffusion coefficient, K, is often given an estimated value due to the difficulty in characterizing the exact processes that contribute to it. TIEGCM uses a value for K computed from Equation 5.3 where Z is the pressure level coordinate TIEGCM uses which ranges from [-7,7] [Wang, 1998].

$$K(z) = 5.0 \times 10^{-6} e^{-7-Z} H_P^2 \tag{5.3}$$

Figure 5.1 shows the values for the molecular diffusion and eddy diffusion coefficients, and it agrees fairly well with Figure 5.2 from the 1976 US Standard Atmosphere.

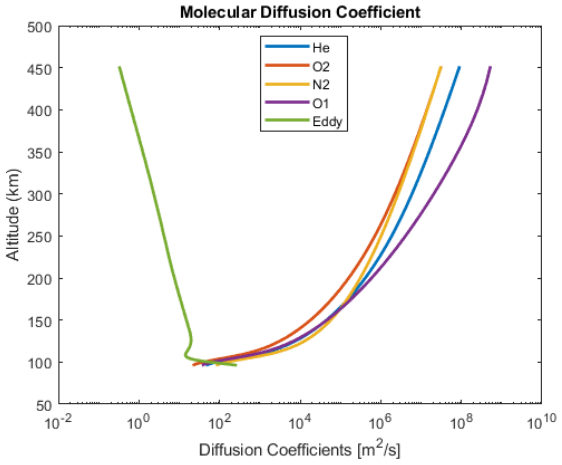

Figure 5.1: Molecular and eddy diffusion coefficients.

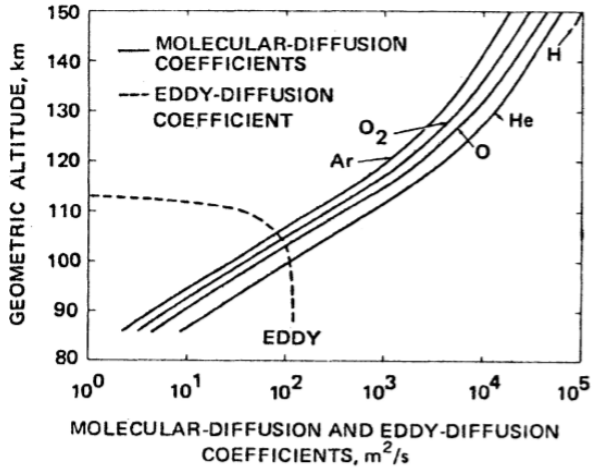

Figure 5.2: Molecular and eddy diffusion coefficients from [Richmond, 1983].

Clearly, eddy diffusion becomes relatively negligible compared to the effects of molecular diffusion above roughly 100km. Above this, viscosity drives eddy diffusion effects down, and molecular diffusion increases due to the lower collision frequencies experienced by the gasses.

5.1 Time Constants

Another common way to examine the importance of the processes is to compare the time constants for the rates at which the processes occur. This involves considering one process at a time, and deriving a characteristic time scale for the process to evolve. The diffusion time constant can be derived from the continuity equation for an individual species shown by Equation 3.1. Taking the vertical component and rearranging the terms yields:

$$\frac{\partial \rho_i}{\partial t} + C_i^z \frac{\partial \rho_i}{\partial z} = -\frac{\partial C_i^z}{\partial z}\rho_i$$

Assuming $U^z = 0$ means that $C_i^z = U_i^z$ and using the definition of the material derivative, the above can be simplified to the ODE in Equation 5.4,

$$\frac{d\rho_i}{dt} = -k(z)\rho_i \tag{5.4}$$

where $k = \frac{\partial C_i^z}{\partial z}$ is substituted in for readability. Now, the time constant for the process can be found in a similar way to finding scale height. Taking the time constant to be the time a value

changes by a factor of $\frac{1}{e}$, then:

$$\tau_i = \rho_i \frac{1}{\frac{d\rho_i}{dt}}$$

which leads to the equation of the time constant in Equation 5.5.

$$\tau = -\frac{1}{\frac{\partial C_i^z}{\partial z}} = \Big(\frac{\partial}{\partial z}\Big[D_i\big(\frac{1}{H_{\rho i}} - \frac{1}{H^*_{\rho i}} - \frac{m_i}{kT}\sum_{t\neq i}\nu_{it}C_t^z\big) + D_{Ti}\frac{1}{H_T} + K\big(\frac{1}{H_\rho} - \frac{1}{H^*_{\rho i}}\big)\Big]\Big)^{-1} \tag{5.5}$$

Now, to evaluate the time constant associated with any one process, the other two are dropped and only the selected process is considered. Additionally, it is common to assume that the diffusion coefficient is independent of z to a first approximation and can then be brought outside of the derivative [Prölss, 2004].

Examining the time constant for molecular diffusion requires evaluating Equation 5.6.

$$\tau_i^{molecular} = \frac{1}{D_i\frac{d}{dz}\big(\frac{1}{H_{\rho i}} - \frac{1}{H^*_{\rho i}}\big)} \tag{5.6}$$

The drag term expressed by $\frac{m_i}{kT}\sum_{t\neq i}\nu_{it}C_t^z$ is assumed to be negligible compared to the effects of the inverse scale height difference and can be dropped. At this point it is convenient to define the derivatives of various scale height values. Distributing the derivative through, it is straightforward to show the relations of 5.7. A more thorough derivation of these equations is given in section A.3 of the appendix.

$$\begin{aligned}
\frac{\partial}{\partial z}\left(\frac{1}{H^*_{\rho i}}\right) &= \frac{1}{{H^*_{\rho i}}^2} - \frac{1}{\rho_i}\frac{\partial^2\rho_i}{\partial z^2}\\
\frac{\partial}{\partial z}\left(\frac{1}{H_T}\right) &= \frac{1}{T}\frac{\partial^2 T}{\partial z^2} - \frac{1}{{H_T}^2}\\
\frac{\partial}{\partial z}\left(\frac{1}{H_{\rho i}}\right) &= -\frac{1}{H_{Pi}}\frac{1}{H_T} - \frac{1}{{H_T}^2} + \frac{1}{T}\frac{\partial^2 T}{\partial z^2}\\
\frac{\partial}{\partial z}\left(\frac{1}{H_\rho}\right) &= \frac{1}{H_P}\left(\frac{1}{H_m} - \frac{1}{H_T}\right) - \frac{1}{H_m^2} - \frac{1}{H_T^2} + \frac{1}{T}\frac{\partial^2 T}{\partial z^2} + \frac{1}{m}\frac{\partial^2 m}{\partial z^2}
\end{aligned} \tag{5.7}$$

By neglecting the second order terms, Equation 5.6 becomes Equation 5.8.

$$\tau_i^{molecular} = \frac{1}{D_i\big(-\frac{m_i g}{kT}\frac{1}{H_T} - \frac{1}{{H_T}^2} - \frac{1}{{H^*_{\rho i}}^2}\big)} = \frac{1}{D_i\big(-\frac{1}{H_T}\frac{1}{H_{\rho i}} - \frac{1}{{H^*_{\rho i}}^2}\big)} \tag{5.8}$$

Equivalent approaches can be made for the thermal and eddy diffusion terms. The resulting in equations are shown in 5.9 and 5.10. D_{Ti} is calculated from $D_{Ti} = \alpha D_i$ where α is equal to -.38.

$$\tau_i^{thermal} = \frac{1}{D_{Ti}\frac{\partial}{\partial z}\left(\frac{1}{H_T}\right)} = \frac{1}{D_{Ti}\left(-\frac{1}{{H_T}^2}\right)} = -\frac{{H_T}^2}{D_{Ti}} \tag{5.9}$$

$$\tau_i^{eddy} = \frac{1}{K\frac{\partial}{\partial z}\left(\frac{1}{H_\rho} - \frac{1}{H_{\rho i}^*}\right)} = \frac{1}{K\left(\frac{1}{H_P}\left[\frac{1}{H_m} - \frac{1}{H_T}\right] - \frac{1}{H_m^2} - \frac{1}{H_T^2} - \frac{1}{{H_{\rho i}^*}^2}\right)} \tag{5.10}$$

Equations 5.8, 5.9, and 5.10 are plotted in Figure 5.3. This is at the Northern helium enhancement

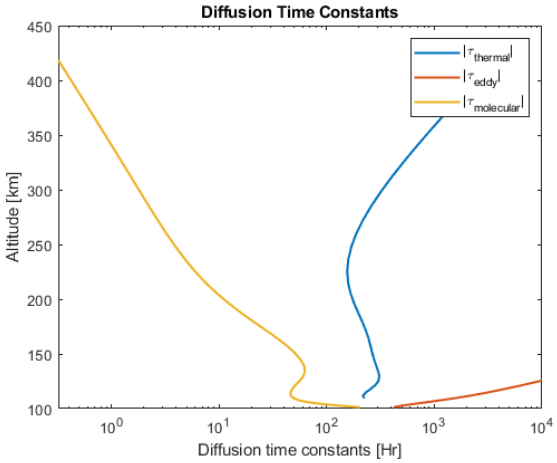

Figure 5.3: Helium diffusion time constants for each process.

region highlighted in Figure 4.2a. The magnitudes of each time constant show that molecular diffusion dominates in the thermosphere. $\tau^{molecular}$ becomes orders of magnitude smaller than the other processes, and at upper altitudes molecular diffusion takes place so rapidly that it is reasonable to neglect the contributions of the other diffusive processes. Thermal diffusion contributes at a small level below around 200km, however as the exospheric temperature is approached the scale height H_T increases dramatically which drives the time constant up. Eddy diffusion becomes negligible very rapidly due to the decreasing K. At 150km the time constant is over three orders of magnitude longer than that of molecular diffusion, indicating a very slow process. It continues to increase with altitude, however the figure cuts this off to maintain an x-axis scale that is meaningful.

It is common to report time constants for processes in terms of $\frac{H^2}{D}$ where H is a scale height for a parameter and D is the diffusion coefficient. This is a result of considering diffusion as purely a Fick's Second Law problem where $\frac{\partial \rho}{\partial t} = D\frac{\partial^2 \rho}{\partial z^2}$. This is what happens for $\tau_i^{thermal}$ where the familiar

form is recovered. When the diffusive process is taken relative to an equilibrium state however, terms such as $-\frac{1}{H_T}\frac{1}{H_{\rho i}} - \frac{1}{H_{\rho i}^{*\,2}}$ appear. This is because a concentration gradient will remain when the species reaches diffusive equilibrium. There is always a gradient present as the total mass density decreases with altitude. Molecular diffusion acts on this gradient, but is balanced by the gravitational and pressure effects. If Fick's Second Law is assumed to be the only constraint, then the vertical concentration gradient would be eliminated, however this does not account for a diffusive equilibrium state.

5.2 Vertical Winds

The final term of equation 3.18 that affects the mass transport in the thermosphere is the vertical wind term. In order to evaluate the extent to which it affects the mass mixing ratio, a different technique can be used. The vertical winds necessary to negate the effects of molecular diffusion can be calculated by setting the time derivative of the mass mixing ratio to zero in Equation 3.18. If molecular diffusion and thermal diffusion are considered the dominant forms of diffusion present, then the eddy diffusion term can be dropped. Arranging the terms results in Equation 5.11.

$$\rho_i w\big(\frac{1}{H_\rho} - \frac{1}{H_{\rho i}^*}\big) = \frac{\partial}{\partial z}\left[\rho_i D_i\big(\frac{1}{H_{\rho i}} - \frac{1}{H_{\rho i}^*}\big) + \rho_i D_{Ti}\frac{1}{H_T}\right] \tag{5.11}$$

Again, pulling the diffusion coefficients out and distributing the derivative produces the intermediate step:

$$\rho_i w\big(\frac{1}{H_\rho} - \frac{1}{H_{\rho i}^*}\big) = D_i\left[\rho_i\big(-\frac{m_i g}{kT}\frac{1}{H_T} - \frac{1}{{H_T}^2} - \frac{1}{H_{\rho i}^{*\,2}}\big) + \frac{\partial \rho_i}{\partial z}\big(\frac{1}{H_{\rho i}} - \frac{1}{H_{\rho i}^*}\big)\right] + D_{Ti}\frac{\partial}{\partial z}\left[\frac{\rho_i}{H_T}\right]$$

When the second order terms are dropped and w is isolated to the left hand side, Equation 5.12 is left.

$$w = -\left(\frac{D_i}{H_{\rho i}} + \frac{D_{Ti}}{H_T}\right)\left(\frac{1}{H_T} + \frac{1}{H_{\rho i}^*}\right)\left(\frac{1}{H_\rho} - \frac{1}{H_{\rho i}^*}\right)^{-1} \tag{5.12}$$

Refer to Section A.4 of the appendix for a detailed derivation of Equation 5.12. As the diffusion coefficients increase with altitude, vertical wind magnitude must as well. Figure 5.4a shows this relationship for helium, again at the location shown in Figure 4.2a. At lower altitudes, vertical

winds can dominate the mass mixing ratio time rate of change, as small winds of tens of meters per second will perturb the time evolution. At higher altitudes however, increasingly large vertical winds are needed to compete with molecular diffusion. It is not common to have vertical winds in the hundreds of meters per second in the upper thermosphere, which the figure shows will effectively compete with molecular diffusion when they oppose each other. This suggests that the effects of vertical winds are limited to the lower regions of the thermosphere. Figure 5.4b shows that the vertical winds from the simulation are very close to the values necessary to compete with molecular diffusion up to nearly 250km. Compared with the necessary vertical winds to balance O_1 diffusion

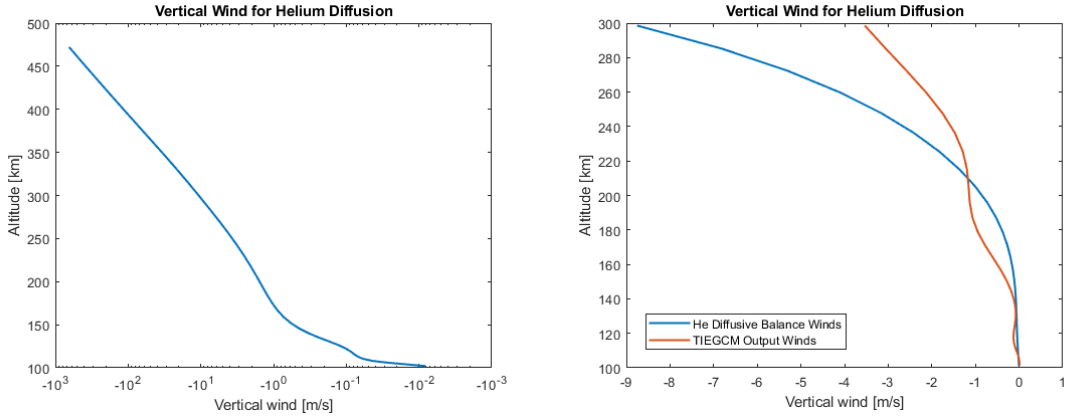

(a) (b)

Figure 5.4: Figure (a) shows the vertical winds necessary to balance molecular diffusion at location 1 (north nighttime helium feature). Figure (b) compares these wind values with the vertical wind output from TIEGCM. TIEGCM run, UT = 0.03hr LT = 6.7hr latitude = 63.75.

seen in Figure 5.5, helium is clearly much more sensitive to vertical winds. O_1 and the other heavier species are very insensitive to vertical winds. At the other locations previously highlighted, the vertical winds act differently, shown in Figure 5.6. At the intermediate helium concentration location, downward winds push the helium scale height to be larger than the diffusive equilibrium profile. On the day side, where the nitrogen concentration peaks at 400km, positive vertical winds act to push the helium scale height to be smaller. At this location, helium closely follows its diffusive profile.

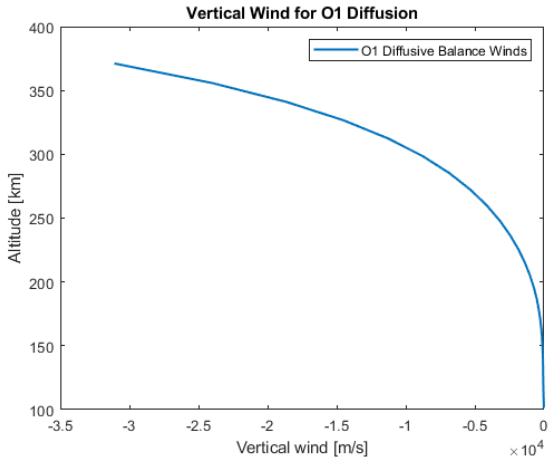

Figure 5.5: Necessary vertical winds to balance O_1 molecular diffusion. TIEGCM run, UT = 0.03hr LT = 6.7hr latitude = 63.75.

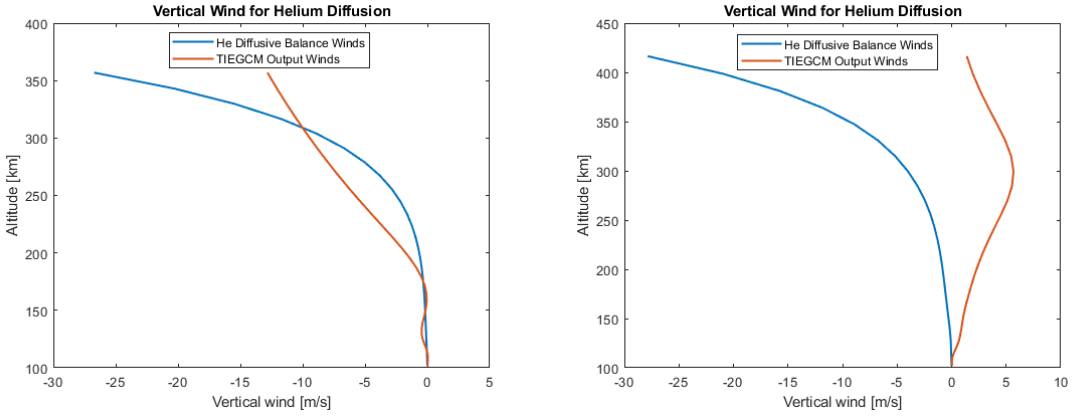

(a) TIEGCM run, UT = 0.03hr LT = 2.7hr latitude = 58.75.

(b) TIEGCM run, UT = 0.03hr LT = 14hr latitude = 11.25.

Figure 5.6: Figure (a) shows the vertical winds necessary to balance molecular diffusion at location 2 (intermediate helium location), along with the TIEGCM output. Figure (b) shows the vertical winds necessary to balance molecular diffusion at location 3 (daytime nitrogen enhancement), along with the TIEGCM output.

Chapter 6

Conclusions and Future Work

The derived mixing ratio transport equation explains the counter intuitive behavior of helium relative to the major species like N_2, O_2, and O_1. The large scale height difference between helium and the total gas make helium transport especially sensitive to vertical winds, and the light molecular weight make it the only neutral species subject to thermal diffusion. The time constant analysis shows that molecular diffusion dominates in the thermosphere, but at lower altitudes thermal diffusion also plays a role. By simplifying the equation using scale heights, a more intuitive understanding of the dynamics can be reached. This understanding will help improve satellite drag estimates and orbit predictions. Also, having a better understanding of the dynamics in the lower thermosphere enhances the ability to model what occurs above the continuum region where this derivation is valid.

Future work should examine the validity of neglecting the $\frac{m_i}{kT}\sum_{t\neq i}\nu_{it}C_t^z$ term in molecular diffusion, as it could play a role that was not considered here. It opens the possibility for a gas species to have zero diffusive flux despite there being a difference in diffusive and actual scale heights. This would be a result of the drag term balancing the diffusive flux towards equilibrium, producing no net flux. Considering this term brings more of the complicated mixed gas dynamics into the derivation, and would enhance the accuracy of the mathematical model.

Additionally, extending the scale height analysis to a three dimensional model could be useful. Diffusion along the horizontal plane might explain further the results of TIEGCM. When uneven

heating over the hemispheres occurs, such as in the solstices, the horizontal transport effects could become significant as features form from converging winds.

Bibliography

Us standard atmosphere, 1976.

Oliver Montenbruck Eberhard Gill. Satellite Orbits. Springer Berlin Heidelberg, 2011. ISBN 978-3-540-67280-7. URL https://www.ebook.de/de/product/1394660/eberhard_gill_oliver_montenbruck_satellite_orbits.html.

Vicki W. Hsu. An Indirect and Dynamically Induced Energy Mechanism in a Plasma-Neutral Atmosphere. PhD thesis, 2016.

Vicki W. Hsu, Jeffrey P. Thayer, Jiuhou Lei, and Wenbin Wang. Formation of the equatorial thermosphere anomaly trough: Local time and solar cycle variations. Journal of Geophysical Research: Space Physics, 119(12):10,456–10,473, dec 2014. doi: 10.1002/2014JA020416.

H. Klinkrad. Space Debris Models and Risk Analysis. Springer-Verlag GmbH, 2006. ISBN 3-540-25448-X. URL https://www.ebook.de/de/product/3198437/h_klinkrad_space_debris_models_and_risk_analysis.html.

Heiner Klinkrad. Large satellite constellations and related challenges for space debris mitigation. Journal of Space Safety Engineering, 4(2):59–60, jun 2017. doi: https://doi.org/10.1016/j.jsse.2017.06.002.

G. Kockarts. Helium in the terrestrial atmosphere, jul 1973.

Xianjing Liu. The Effects of Composition on Thermosphere Mass Density Response to Geomagnetic Activity. PhD thesis, 2013.

J. M. Picone, A. E. Hedin, D. P. Drob, and A. C. Aikin. NRLMSISE-00 empirical model of the atmosphere: Statistical comparisons and scientific issues. Journal of Geophysical Research: Space Physics, 107(A12):SIA 15–1–SIA 15–16, dec 2002. doi: 10.1029/2002JA009430.

David Mostaza Prieto, Benjamin P. Graziano, and Peter C. E. Roberts. Spacecraft drag modelling. Progress in Aerospace Sciences, 64:56–65, jan 2014. doi: https://doi.org/10.1016/j.paerosci.2013.09.001.

Gerd Prölss. Physics of the Earth's Space Environment: An Introduction. Springer, 2004. ISBN 3-540-21426-7. URL https://www.amazon.com/Physics-Earths-Space-Environment-Introduction/dp/3540214267?SubscriptionId=AKIAIOBINVZYXZQZ2U3A&tag=chimbori05-20&linkCode=xm2&camp=2025&creative=165953&creativeASIN=3540214267.

Jonas Radtke, Christopher Kebschull, and Enrico Stoll. Interactions of the space debris environment with mega constellations—using the example of the OneWeb constellation. Acta Astronautica, 131:55–68, feb 2017. doi: https://doi.org/10.1016/j.actaastro.2016.11.021.

Arthur D. Richmond. Thermospheric dynamics and electrodynamics. In R. L. Carovillano and J. M. Forbes, editors, Solar-Terrestrial Physics, pages 523–607. Springer Netherlands, 1983. doi: http://dx.doi.org/10.1007/978-94-009-7194-3.

Robert W. Schunk and Andrew F. Nagy. Ionospheres - Physics, Plasma Physics, and Chemistry. Cambridge University Press, 2000. ISBN 0521607701.

Eric K. Sutton, Jeffrey P. Thayer, Wenbin Wang, Stanley C. Solomon, Xianjing Liu, and Benjamin T. Foster. A self-consistent model of helium in the thermosphere. Journal of Geophysical Research: Space Physics, 120(8):6884–6900, aug 2015. doi: 10.1002/2015JA021223.

Wenbin Wang. A Thermosphere-Ionosphere Nested Grid (TING) Model. PhD thesis, 1998.

Nomenclature

$\frac{\rho_i}{\rho}$	Mass mixing ratio
Γ_i	Diffusive mass flux
λ	Molecular mean free path
ν_{it}	Momentum weighted collision frequency
ρ	Total atmospheric gas mass density
ρ_i	Individual gas species mass density
σ	Sum of the radii of colliding molecules
$\vec{C_i} = \left(\vec{U_i} - \vec{U}\right)$	Diffusion velocity of gas species i
$\vec{U_i}$	Individual species mean velocity
$\vec{U}$	Mass averaged velocity
C_D	Coefficient of drag
$D_i = \frac{kT}{\sum_{t \neq i} m_i \nu_{it}}$	Molecular diffusion coefficient
D_{Ti}	Thermal diffusion coefficient
K	Eddy diffusion coefficient
k	Boltzmann's constant

Kn	Knudsen number
L	Characteristic length
m_i	Molecular weight of species 'i'
P_i	Partial pressure of species 'i'
T	Temperature

Appendix A

Derivations

A.1 Diffusive Flux

This derivation deviates from the derivation of Liu [2013] as shown:

Beginning with Equation 1.7 from Liu's thesis:

$$\nabla P_i - n_i m_i \vec{G} = -n_i m_i \sum_{t \neq i} \nu_{it}(\vec{C}_i - \vec{C}_t) \tag{A.1}$$

Simplify $n_i m_i$ to ρ_i:

$$\nabla P_i - \rho_i \vec{G} = -\rho_i \sum_{t \neq i} \nu_{it}(\vec{C}_i - \vec{C}_t) \tag{A.2}$$

Divide through by $-\rho_i$:

$$-\frac{1}{\rho_i}\big(\nabla P_i - \rho_i \vec{G}\big) = \sum_{t \neq i} \nu_{it}(\vec{C}_i - \vec{C}_t) \tag{A.3}$$

Separate the summation term on the right hand side:

$$-\frac{1}{\rho_i}\big(\nabla P_i - \rho_i \vec{G}\big) = \sum_{t \neq i} \nu_{it}\vec{C}_i - \sum_{t \neq i} \nu_{it}\vec{C}_t \tag{A.4}$$

Add $\sum_{t \neq i} \nu_{it}\vec{C}_t$ to both sides:

$$-\frac{1}{\rho_i}\big(\nabla P_i - \rho_i \vec{G}\big) + \sum_{t \neq i} \nu_{it}\vec{C}_t = \sum_{t \neq i} \nu_{it}\vec{C}_i \tag{A.5}$$

Bring the $\sum_{t \neq i} \nu_{it}\vec{C}_t$ term into the parentheses on the left hand side:

$$-\frac{1}{\rho_i}\big(\nabla P_i - \rho_i \vec{G} - \rho_i \sum_{t \neq i} \nu_{it}\vec{C}_t\big) = \sum_{t \neq i} \nu_{it}\vec{C}_i \tag{A.6}$$

Divide through by $\sum_{t\neq i}\nu_{it}$:

$$\vec{C_i} = -\frac{1}{\rho_i \sum_{t\neq i}\nu_{it}}\left(\nabla P_i - \rho_i\vec{G} - \rho_i\sum_{t\neq i}\nu_{it}\vec{C_t}\right) \tag{A.7}$$

Express diffusive flux by multiplying both sides by ρ_i:

$$\vec{\Gamma}_{Di} = \rho_i\vec{C_i} = -\frac{1}{\sum_{t\neq i}\nu_{it}}\left(\nabla P_i - \rho_i\vec{G} - \rho_i\sum_{t\neq i}\nu_{it}\vec{C_t}\right) \tag{A.8}$$

Equation A.8 differs from equation 1.8 in Liu's thesis which is shown below by a sign change on the $\rho_i\sum_{t\neq i}\nu_{it}\vec{C_t}$ term:

$$\vec{\Gamma}_{Di} = \rho_i\vec{C_i} = -\frac{1}{\sum_{t\neq i}\nu_{it}}\left(\nabla P_i - \rho_i\vec{G} + \rho_i\sum_{t\neq i}\nu_{it}\vec{C_t}\right) \tag{A.9}$$

A.2 Error Analysis

Finding "Scale Height", or λ, from data by fitting an exponential curve to the data introduces some error for data that does not follow an exponential profile. In this derivation, λ refers to the actual scale height, while λ^* is the derived approximation for the exact value. Let the data points, x_1, x_2, and x_3 have corresponding y values of y_1, y_2, and y_3 respectively. Assume an exponential profile around (x_2, y_2) constructed such that $f(x) = y_2 e^{\frac{x-x_2}{\lambda}}$ and $f(x_2) = y_2$ and $f'(x_2) = y_2'$. The other values, y_1 and y_2 follow the exponential but with an adjustment factor. So, $y_1 = f(x_1)\eta, \quad y_3 = f(x_3)\delta$ for $0 \leq \eta, \delta \leq \infty$. Then consider:

$$ln(y_1) = ln(f(x_1)\eta) = ln(f(x_1)) + ln(\eta) = ln(y_2 e^{\frac{x1-x2}{\lambda}}) + ln(\eta) = ln(y_2) + \frac{x_1 - x_2}{\lambda} + ln(\eta)$$

$$ln(y_3) = ln(f(x_3)\delta) = ln(f(x_3)) + ln(\delta) = ln(y_2 e^{\frac{x3-x2}{\lambda}}) + ln(\delta) = ln(y_2) + \frac{x_3 - x_2}{\lambda} + ln(\delta)$$

Calculating λ^* by assuming an exponential profile for y can then summarized by Equation A.10.

$$\frac{1}{\lambda^*} = \frac{ln(y_3) - ln(y_1)}{x_3 - x_1} \tag{A.10}$$

Then:

$$\frac{1}{\lambda^*} = \frac{ln(y_2) + \frac{x_3-x_2}{\lambda} + ln(\delta) - ln(y_2) - \frac{x_1-x_2}{\lambda} - ln(\eta)}{x_3 - x_1} = \frac{\frac{x_3-x_1}{\lambda} + ln(\delta) - ln(\eta)}{x_3 - x_1}$$

Simplifying:

$$\frac{1}{\lambda^*} = \frac{1}{\lambda} + \frac{ln(\frac{\delta}{\eta})}{x_3 - x_1} \tag{A.11}$$

Solving for λ^* we get the following:

$$\lambda^* = \frac{\lambda(x_3 - x_1)}{(x_3 - x_1) + \lambda ln(\frac{\delta}{\eta})} \tag{A.12}$$

Thus the error term, $(\lambda ln(\frac{\delta}{\eta}))$, is in the denominator. If δ and η are both equal to 1, then the error term is zero and equation A.12 simplifies to just $\lambda^* = \lambda$. If they are both close to 1 then the error is extremely small. The following plots for Helium show that the values of $f(x_1)$, $f(x_3)$ and y_1, y_3 are respectively very close and therefore the error can be neglected. Note, all plots are made using Hsu's TIEGCM run `HSUVW.tiegcm2.0_dres.pdrag_f107_180_001.nc` at latitude of 61.25 deg and longitude of 97.5 deg.

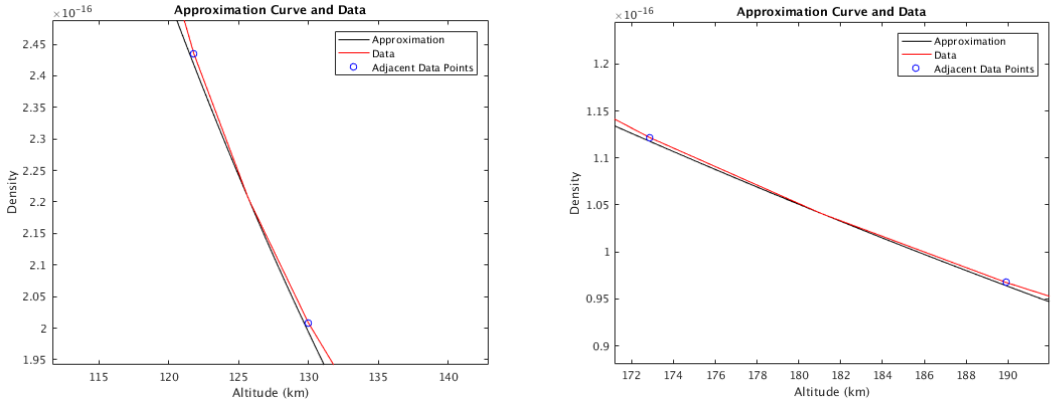

(a)

(b)

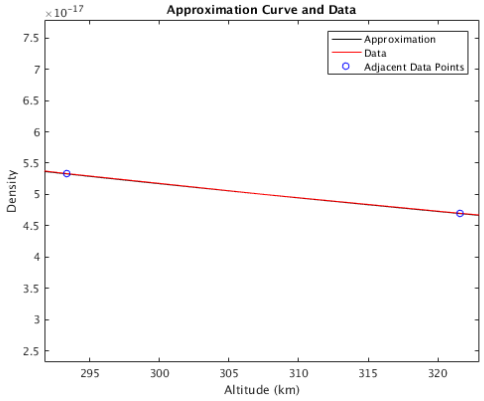

(c)

Figure A.1: Error associated with using the exponential assumption.

As altitude increases the density more closely follows an exponential profile and therefore the approximation and data curves match very well. At an altitude of 125km the approximation and data curves diverge, but in amounts that render the error in λ negligible. At higher altitudes, η and δ become increasingly close to 1, dominating the error term in the denominator of equation A.12 even though λ increases. As a check, the error term in the denominator amounts to a value on the order of 10^{-5}km at the 125km altitude. This is a negligible addition when $|x_1 - x_3|$ at this

altitude is roughly 8km. From these results, using an exponential curve fit to the data is accurate for these purposes.

This works well because a previous three-point differentiation scheme was originally used, however it was found that there was a consistent bias made to the scale height plots. The exponential method shown here produced better results that were tested against the total density profile. TIEGCM imposes hydrostatic equilibrium on the total gas, therefore the calculated scale height should match the equilibrium scale height. The results are shown in Figure A.2.

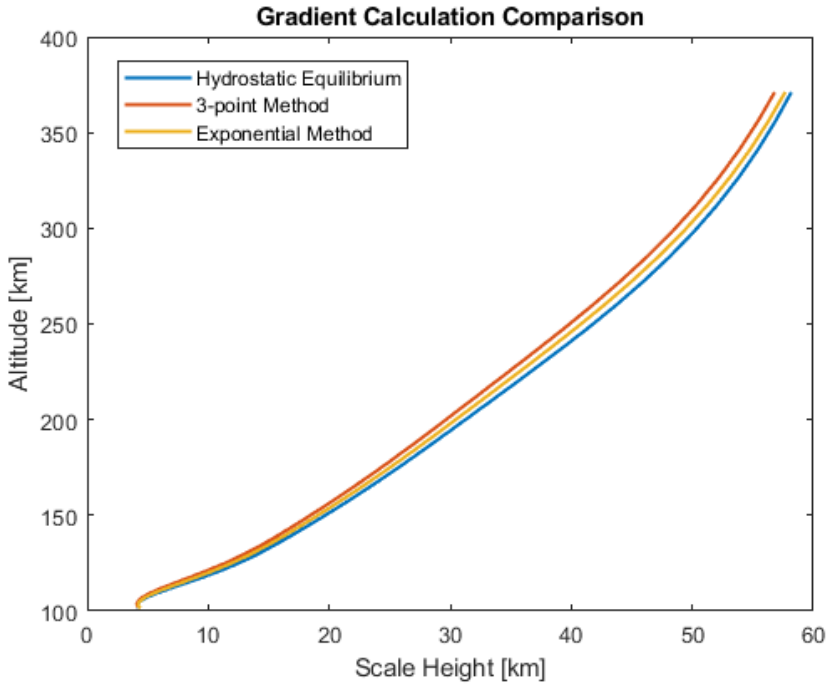

Figure A.2: Comparison of the exponential method and three point differentiation method against hydrostatic equilibrium.

A.3 Equations 5.7

The equations presented in 5.7 are derived here:

1)

$$\frac{\partial}{\partial z}\left(\frac{1}{H^*_{\rho i}}\right) = \frac{\partial}{\partial z}\left(-\frac{1}{\rho_i}\frac{\partial \rho_i}{\partial z}\right) = -\frac{1}{\rho_i}\frac{\partial^2 \rho_i}{\partial z^2} - \frac{\partial \rho_i}{\partial z}\left(-\frac{1}{\rho_i^2}\frac{\partial \rho_i}{\partial z}\right) = \frac{1}{{H^*_{\rho i}}^2} - \frac{1}{\rho_i}\frac{\partial^2 \rho_i}{\partial z^2} \tag{A.13}$$

2)

$$\begin{aligned} \frac{\partial}{\partial z}\left(\frac{1}{H_T}\right) &= \frac{\partial}{\partial z}\left(\frac{1}{T}\frac{\partial T}{\partial z}\right) = \frac{1}{T}\frac{\partial^2 T}{\partial z^2} + \frac{\partial T}{\partial z}\frac{\partial}{\partial z}\left(\frac{1}{T}\right) \\ \frac{\partial}{\partial z}\left(\frac{1}{H_T}\right) &= \frac{1}{T}\frac{\partial^2 T}{\partial z^2} - \frac{1}{T^2}\left(\frac{\partial T}{\partial z}\right)^2 = \frac{1}{T}\frac{\partial^2 T}{\partial z^2} - \frac{1}{H_T^2} \end{aligned} \tag{A.14}$$

3)

$$\begin{aligned} \frac{\partial}{\partial z}\left(\frac{1}{H_{\rho i}}\right) &= \frac{\partial}{\partial z}\left(\frac{1}{H_{Pi}} + \frac{1}{H_T}\right) = \frac{\partial}{\partial z}\left(\frac{m_i g}{kT} + \frac{1}{H_T}\right) \\ &= \frac{m_i g}{k}\frac{\partial}{\partial z}\left(\frac{1}{T}\right) + \frac{\partial}{\partial z}\left(\frac{1}{T}\frac{\partial T}{\partial z}\right) = -\frac{m_i g}{k}\frac{1}{T^2}\frac{\partial T}{\partial z} + \left(\frac{1}{T}\frac{\partial^2 T}{\partial z^2} - \frac{1}{{H_T}^2}\right) \\ \frac{\partial}{\partial z}\left(\frac{1}{H_{\rho i}}\right) &= -\frac{m_i g}{kT}\frac{1}{H_T} - \frac{1}{{H_T}^2} + \frac{1}{T}\frac{\partial^2 T}{\partial z^2} \end{aligned} \tag{A.15}$$

4)

$$\begin{aligned} \frac{\partial}{\partial z}\left(\frac{1}{H_\rho}\right) &= \frac{\partial}{\partial z}\left(\frac{1}{H_P} + \frac{1}{H_m} + \frac{1}{H_T}\right) = \frac{\partial}{\partial z}\left(\frac{mg}{kT} + \frac{1}{H_m} + \frac{1}{H_T}\right) \\ &= \frac{g}{k}\frac{\partial}{\partial z}\left(\frac{m}{T}\right) - \frac{1}{H_m^2} - \frac{1}{H_T^2} + \frac{1}{T}\frac{\partial^2 T}{\partial z^2} + \frac{1}{m}\frac{\partial^2 m}{\partial z^2} \\ &= \frac{g}{kT}\frac{\partial m}{\partial z} - \frac{mg}{kT}\frac{1}{T}\frac{\partial T}{\partial z} - \frac{1}{H_m^2} - \frac{1}{H_T^2} + \frac{1}{T}\frac{\partial^2 T}{\partial z^2} + \frac{1}{m}\frac{\partial^2 m}{\partial z^2} \\ &= \frac{mg}{kT}\frac{1}{H_m} - \frac{mg}{kT}\frac{1}{H_T} - \frac{1}{H_m^2} - \frac{1}{H_T^2} + \frac{1}{T}\frac{\partial^2 T}{\partial z^2} + \frac{1}{m}\frac{\partial^2 m}{\partial z^2} \\ \frac{\partial}{\partial z}\left(\frac{1}{H_\rho}\right) &= \frac{mg}{kT}\left(\frac{1}{H_m} - \frac{1}{H_T}\right) - \frac{1}{H_m^2} - \frac{1}{H_T^2} + \frac{1}{T}\frac{\partial^2 T}{\partial z^2} + \frac{1}{m}\frac{\partial^2 m}{\partial z^2} \end{aligned} \tag{A.16}$$

A.4 Equation 5.12

Starting with Equation 5.11 below, Equation 5.12 will be derived.

Equation 5.11:

$$\rho_i w\left(\frac{1}{H_\rho} - \frac{1}{H^*_{\rho i}}\right) = \frac{\partial}{\partial z}\left[\rho_i D_i\left(\frac{1}{H_{\rho i}} - \frac{1}{H^*_{\rho i}}\right) + \rho_i D_{Ti}\frac{1}{H_T}\right] \tag{A.17}$$

Pull the diffusion coefficients outside of the derivative, and distribute the derivative using the product rule:

$$\begin{aligned}\rho_i w\big(\frac{1}{H_\rho}-\frac{1}{H^*_{\rho i}}\big) &= D_i\bigg[\rho_i\frac{\partial}{\partial z}\big(\frac{1}{H_{\rho i}}-\frac{1}{H^*_{\rho i}}\big)+\frac{\partial\rho_i}{\partial z}\big(\frac{1}{H_{\rho i}}-\frac{1}{H^*_{\rho i}}\big)\bigg]+D_{Ti}\frac{\partial}{\partial z}\bigg(\rho_i\frac{1}{H_T}\bigg)\\ &= D_i\bigg[\rho_i\frac{\partial}{\partial z}\big(\frac{1}{H_{\rho i}}-\frac{1}{H^*_{\rho i}}\big)+\frac{\partial\rho_i}{\partial z}\big(\frac{1}{H_{\rho i}}-\frac{1}{H^*_{\rho i}}\big)\bigg]+D_{Ti}\bigg(-\rho_i\frac{1}{H_T^2}+\frac{1}{H_T}\frac{\partial\rho_i}{\partial z}\bigg)\end{aligned} \tag{A.18}$$

Now divide through by ρ_i:

$$\begin{aligned}w\big(\frac{1}{H_\rho}-\frac{1}{H^*_{\rho i}}\big) &= D_i\bigg[\frac{\partial}{\partial z}\big(\frac{1}{H_{\rho i}}-\frac{1}{H^*_{\rho i}}\big)+\frac{1}{\rho_i}\frac{\partial\rho_i}{\partial z}\big(\frac{1}{H_{\rho i}}-\frac{1}{H^*_{\rho i}}\big)\bigg]+D_{Ti}\bigg(-\frac{1}{H_T^2}+\frac{1}{H_T}\frac{1}{\rho_i}\frac{\partial\rho_i}{\partial z}\bigg)\\ &= D_i\bigg[\frac{\partial}{\partial z}\big(\frac{1}{H_{\rho i}}-\frac{1}{H^*_{\rho i}}\big)-\frac{1}{H^*_{\rho i}}\big(\frac{1}{H_{\rho i}}-\frac{1}{H^*_{\rho i}}\big)\bigg]+D_{Ti}\bigg(-\frac{1}{H_T^2}-\frac{1}{H_T}\frac{1}{H^*_{\rho i}}\bigg)\\ &= D_i\bigg(-\frac{m_ig}{kT}\frac{1}{H_T}-\frac{1}{{H_T}^2}-\frac{1}{{H^*_{\rho i}}^2}+\frac{1}{{H^*_{\rho i}}^2}-\frac{1}{H^*_{\rho i}}\frac{1}{H_{\rho i}}\bigg)\\ &\qquad +D_{Ti}\bigg(-\frac{1}{H_T^2}-\frac{1}{H_T}\frac{1}{H^*_{\rho i}}\bigg)\\ &= D_i\bigg[-\frac{1}{H_T}\big(\frac{m_ig}{kT}+\frac{1}{H_T}\big)-\frac{1}{H^*_{\rho i}}\frac{1}{H_{\rho i}}\bigg]+D_{Ti}\bigg(-\frac{1}{H_T^2}-\frac{1}{H_T}\frac{1}{H^*_{\rho i}}\bigg)\\ &= D_i\bigg[-\frac{1}{H_T}\frac{1}{H_{\rho i}}-\frac{1}{H^*_{\rho i}}\frac{1}{H_{\rho i}}\bigg]+D_{Ti}\bigg(-\frac{1}{H_T^2}-\frac{1}{H_T}\frac{1}{H^*_{\rho i}}\bigg)\\ w\big(\frac{1}{H_\rho}-\frac{1}{H^*_{\rho i}}\big) &= -\frac{D_i}{H_{\rho i}}\bigg(\frac{1}{H_T}+\frac{1}{H^*_{\rho i}}\bigg)-\frac{D_{Ti}}{H_T}\bigg(\frac{1}{H_T}+\frac{1}{H^*_{\rho i}}\bigg)\end{aligned} \tag{A.19}$$

Finally, isolating w to one side produces Equation 5.12 shown below:

$$w=-\bigg(\frac{D_i}{H_{\rho i}}+\frac{D_{Ti}}{H_T}\bigg)\bigg(\frac{1}{H_T}+\frac{1}{H^*_{\rho i}}\bigg)\bigg(\frac{1}{H_\rho}-\frac{1}{H^*_{\rho i}}\bigg)^{-1} \tag{A.20}$$